Angular Spread Measurement and Modeling for 3D MIMO in Urban Macrocellular Radio Channels

Jiao Wang[1], Ruonan Zhang[1], Weiming Duan[2], Stan X. Lu[2], and Lin Cai[3]
[1]Northwestern Polytechnical University, Xi'an, Shaanxi, China
[2]Huawei Technologies Ltd., Xi'an, Shaanxi, China
[3]University of Victoria, Victoria, British Columbia, Canada

***Abstract*—When planar antenna arrays are introduced at the base stations (BSs) of cellular networks, accurate modeling of the spatial radio channel in there-dimension (3D) will become crucial. In this paper, a field measurement campaign was conducted to characterize the 3D spatial propagation to the BS in urban street canyon environments. Using a wideband channel sounder with two uniform planar antenna arrays, the angular spread (AS) in both azimuth and elevation domains at the BS was measured with the user equipment (UE) located at 100 different positions in LOS scenario and 95 positions in NLOS scenario. Contrary to the expected simple correlation between the large-scale fading (like path loss) and AS, our measurements have shown much more complicated relationship between AS and the surrounding environment. It is demonstrated that, in LOS scenario, the AS has positive correlation with the UE-to-BS distance in wide street, but negative correlation in narrow street. In NLOS scenario, the correlation between AS and the transceiver distance is positive when the UE is too close to a building to have "Quasi-LOS" path (diffracted over the building roof) propagation. However, if "Quasi-LOS" path is strengthened, the correlation is reversed. These observations lead to the need of more sophisticated models on the angular characteristics in urban radio channels. Based on the collected data, we also present the Laplacian distribution models of AS in both azimuth and elevation domains.**

I. Introduction

By space division multiple access (SDMA), multiple user equipments (UEs) at different locations may communicate with the base station (BS) simultaneously. In the next generation cellular systems, BS will employ planar antenna array instead of the current linear array. Thus, it becomes possible to utilize the spatial properties of the three-dimensional (3D) multiple-input multiple-output (MIMO) wireless channel to further improve the spectral efficiency and system capacity. Therefore, characterizing the 3D multipath channels concerning the angular spread (AS) of power departure and arrival would be critical to exploit the spatial multiplexing in 3D MIMO systems.

Current 2D MIMO channel models as proposed in 3GPP TR25.996 [1] and WINNER reports [2] have been widely adopted as references for the development of cellular wireless systems. However, they have only standardized the MIMO channel models in azimuth domain, such as azimuth RMS spread of arrival (ASA), leaving the spatial model and parameters in elevation domain undetermined. In the literature, the practical measurements have been carried out to characterize the 3D spatial propagation on the UE side at street level [3], [4]. The autocorrelation function of AS has been studied in [5]. In addition, the elevation characteristics, such as elevation RMS spread of arrival (ESA), extracted from measurements have been reported in literature [6]–[8]. However, these models only focus on the elevation characteristics, rather than estimating angle-of-arrival in both azimuth and elevation jointly. More importantly, the spatial propagation characteristics on the BS side when the UE is located at different places are still ignored. In order to study and fully utilize the 3D MIMO, channel statistics and models on the BS side are needed, which has motivated this work.

Since realistic models require channel measurements to prove their descriptions and enable appropriate parameter selection, the main objective of this paper is to perform field measurements on the 3D angular power arrival on the BS side and establish the relationship of ASA and ESA with the propagation environment.

The main contributions of this paper are three fold. Firstly, a measurement campaign on the 3D radio channel in typical urban street canyons was carried out by the joint effort of Northwestern Polytechnical University (NPU) and Huawei Technologies Ltd. The BS was installed on the top of a 5-floor building and the UE was moving on rectangular grids along two streets with line-of-sight (LOS) and none-line-of-sight (NLOS), respectively. According to 3GPP [1], they are defined as typical pedestrian business street in modern urban macro cell (UMa) areas. The 3D channel sounding was realized by two uniform planar array (UPA) antennas, each with 32 dual-polarized dipole elements, and a complex wideband radio channel sounder. The receiver UPA can provide the amplitude and phase information of the array signals in horizontal and vertical planes. Totally 100 LOS and 95 NLOS locations were measured with 2.6 GHZ central frequency and 62.5 MHZ bandwidth. Secondly, the multipath channel impulse responses (CIRs) were extracted from the captured waveforms and, using an iterative 2-dimensional MUSIC algorithm, the incident angle of each individual propagation path was jointly estimated in azimuth and elevation domains. Based on the 3D angular power arrival distribution, the ASA and ESA for all the UE locations were obtained. Finally, the correlation of ASA and ESA with the transceiver distance and surrounding environment was analyzed based on the collected data. The Laplacian distribution model was also presented.

This work helps to reveal the 3D propagation in UMa radio channels and improve the applicability of the ITU spatial channel models in realistic 3D channel simulations.

The rest of the paper is organized as follows. Section II describes the 3D channel sounder, the measurement setup. The measurement results including extracted CIRs and AS

978-1-4799-4640-2/14/$31.00 ©2014 IEEE

Fig. 1. 3D channel sounder (left: BS, Rx system; right: UE, Tx system)

are presented in Section III. The statistical model of AS is proposed in Section IV. Section V concludes the paper and points out the future research issues.

II. Measurement Scenarios

The measurements were conducted on the campus of NPU in the suburb of Xi'an, China. We selected two streets for LOS and NLOS scenarios, respectively, which are typical street canyons in UMa in the 3GPP standard [1].

A. Measurement System

We used the wideband channel sounder developed by Huawei and NPU as shown in Fig. 1 to perform the 3D channel measurement. The Tx and Rx systems were placed in two movable cabinets. Two UPA antennas were mounted on top of the cabinets so that their centers were at height of 2.09 m above ground level. A UPA was composed of 16 patches each of which contained 2 dipole elements of $\pm 45^o$ polarizations, 7 dBi gain and 90^o beamwidth on both horizontal and vertical planes. The photographs of the two UPAs can also been seen in Fig. 1. The spacings between the adjacent patches are 0.5 wavelength. Two GPS-triggered rubidium clocks provided the synchronized clocks to the Tx and Rx such that synchronized 1 pulse per second (PPS) clocks on both sides started the signal generation and capture at the same time.

In the Tx, cyclic pseudo-noise sequences modulated the carrier of 2.6 GHz by BPSK. An M-sequence with 1023 chips was chosen and the chip frequency was 62.5 MHz leading to a delay resolution of 16 ns. In the Rx, the 4 elements with $+45^o$ polarization on the 4 patches in the first row of the UPA formed a uniform linear array (ULA) in the horizontal dimension (we focus on a single polarization in this paper). Similarly, the 4 $+45^o$ polarized elements on the 4 patches in second column formed a vertical ULA. Thus the angle-of-arrival in the azimuth and elevation domains could be measured, respectively.

B. LOS Scenario

The BS was installed on the top of a 5-floor building, as shown in Fig. 1 (left). The photograph of the street for LOS scenario taken from the BS is shown in Fig. 2. As mentioned earlier, because 3D MIMO antenna system is expected to be mounted on the BS, we used the Rx as BS and the

Fig. 2. Photograph of the street for UMa LOS Scenario.

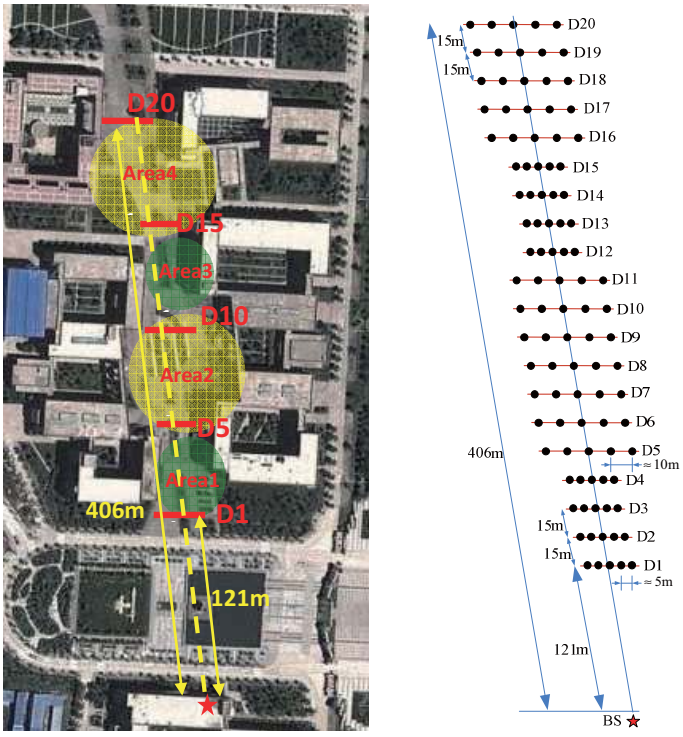

Fig. 3. Measurement positions in the street for UMa LOS Scenario.

Tx as UE in order to measurement the angle-of-arrival and characterize the spatial parameters at the BS. The height of the center of the BS UPA antenna was 24.5 meters. The UE was moved on a rectangular grid along the street, as illustrated in Fig. 3. 5 positions were arranged on a line at the same distance and totally 100 positions were measured on 20 lines at different distances. The distance between the BS and UE (D_1, D_2, $\cdots$, D_{20}) is annotated in Fig. 3(b). The UE setup is shown in Fig. 1 (right).

For each UE location, the 32 antenna elements (as presented in Section II-A, including $\pm 45^o$) on the UPA transmitted sequentially for two rounds. In one round, the horizontal ULA on the Rx was connected to the oscilloscope for array signal capture. Then in the other round, the signals on the vertical ULA were captured . Thus, we recorded totally 64 array signals for four categories, *i.e.*, two polarization directions ($\pm 45^o$) and two dimensions (azimuth and elevation). Since a ULA was composed of 4 elements, one array signal included 4

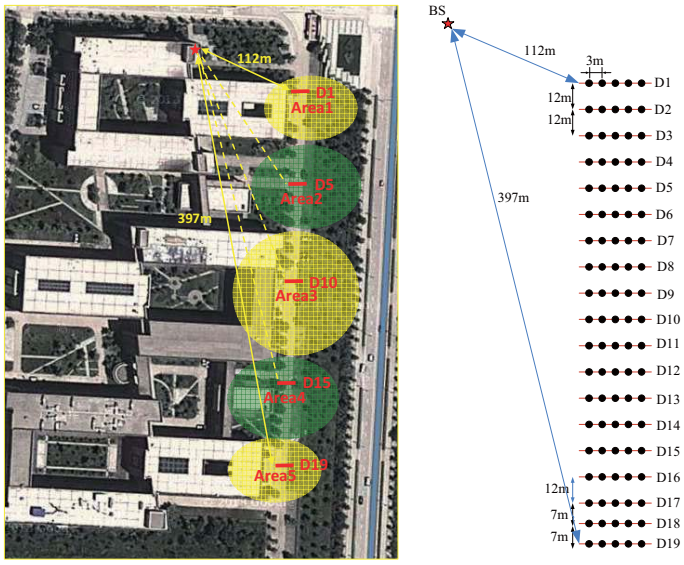

Fig. 4. Measurement positions in the street for UMa NLOS Scenario. (Red star marks the position of BS.)

channel response waveforms. Therefore, at each UE location, the 16 array signals would provide 64 samples of CIRs and 16 samples of angular arrival distribution for one polarization and one dimension.

C. NLOS Scenario

The BS was installed on the top of the same building but the UE was moved on another street with NLOS propagation obstructed by other buildings. The UE positions were arranged on a rectangular grid along the street and totally 95 positions were measured, as illustrated in Fig. 4. The measurement method was the same as in the LOS scenario.

III. Measurement Results

A. Overview

With the objective of investigating the 3D spatial propagation in radio channels, we propose a statistical baseband model which incorporates time-of-arrival (ToA), azimuth angle-of-arrival (AoA) and elevation angle-of-arrival (EoA) information. The combined impulse response is expressed as

$$h(t,\phi,\theta) = \Sigma_{k=1}^{K} \alpha_k e^{j\psi_k} \delta(t-\tau_k)\delta(\phi-\varphi_k)\delta(\theta-\vartheta_k), \quad (1)$$

where K is the number of resolvable paths, $\alpha_k e^{j\psi_k}$, τ_k, φ_k and ϑ_k are the complex gain, ToA, AoA and EoA of the k-th path, respectively. α_k and ψ_k are the gain and phase shift introduced by the propagation of the path. The model in (1) is a simplified version of that for indoor ToA and AoA proposed in [9], where the arrivals are modeled to be clustered in both time and azimuth domains. The clustered arrivals were also observed in time, azimuth and elevation domains in our measurement. Due to the space limit, we focus on the main cluster in azimuth and elevation domains in this paper. The spatial clustering statistics will be further studied in our future works with more measurement data available.

The time-domain multipath CIRs were extracted and $\alpha_k e^{j\psi_k}$ and τ_k were obtained from each captured waveforms, as briefly presented in Section II-A. For each distinguished path in the extracted CIRs, its AoA and EoA, *i.e.*, φ_k and ϑ_k, were jointly estimated using two-dimensional MUSIC algorithm [10]. Then the angular power distribution in the azimuth and elevation domains was obtained for each array signal sample. As mentioned in Section II, we obtained 16 samples of array signals for one polarization and one dimension. Thus, we got 16 samples of the angular arrival distributions, each corresponding to a Tx element.

Based on the AoA and EoA information extracted from the CIRs, the angular power spectrum (APS) which is the distribution of power arrival over the incident angles can be obtained in the two dimensions. The angular spread (AS) is an important parameter to describe not only the angle-of-arrival of the rays but also spatial distribution of the incident power. The AS in elevation domain, ESA, is defined as

$$ESA = \sqrt{\frac{\sum_{k=1}^{K}\left(\vartheta_k - \mu_{APS}\right)^2 \alpha_k^2}{\sum_{k=1}^{K}\alpha_k^2}}, \quad (2)$$

where μ_{APS} is the mean APS and is calculated by

$$\mu_{APS} = \frac{\sum_{k=1}^{K}\vartheta_k \alpha_k^2}{\sum_{k=1}^{K}\alpha_k^2}. \quad (3)$$

The AS in azimuth domain, ASA, is defined similarly by replacing ϑ_k by φ_k in (2) and (3).

Since we obtained 16 samples of APS in one dimension for each UE position, we had totally $16 \times 5 = 80$ samples of ASA and ESA on the 5 positions of one distance.

The mean value and standard deviation (STD) of the 80 samples of ASA and ESA at each UE distance are plotted in Fig. 5 and 6. We can see that both curves run zigzag with the increase of UE distance. Interesting observations are found, as discussed in details in the following subsections.

B. ASA and ESA in LOS Scenario

As shown in the map in Fig. 3, the width of the measurement street is actually changing due to the irregular layout of the buildings on the two sides. Along the position grid of the UE, we can divide the street into 4 areas according to its width, as illustrated in Fig. 3. The street width of *Area1* and *Area3* is about 27m, while the width of *Area2* and *Area4* is about 55m, much wider than the former two areas.

It can be seen that the variation tendency of ASA and ESA in Fig. 5 matches the change of the street width. Specifically speaking, when the UE was moved in *Area1* (distance between 121m and 180m) and *Area3* (distance between 286m and 346m), ASA and ESA basically decrease with the increase of the UE-to-BS distance. When the UE was moved in *Area2* (distance between 180m and 286m) and *Area4* (distance between 346m and 406m), ASA and ESA basically increase with the distance. For easy presentation, the areas with the same ASA/ESA tendency are called *homogeneous areas*. In

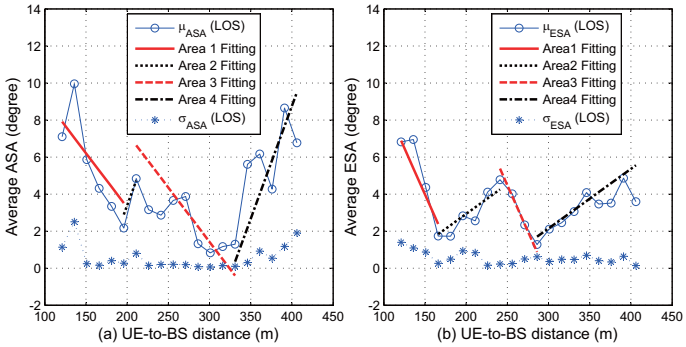

Fig. 5. Spatial parameters from field LOS measurements.

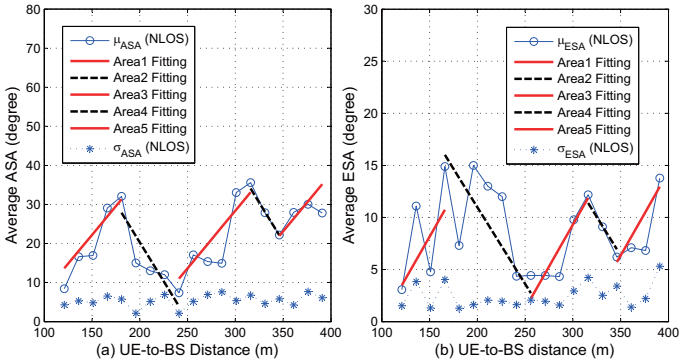

Fig. 6. Spatial parameters from field NLOS measurements.

addition, it can also be seen that the fluctuation of ASA and ESA is coincident with each other.

The coincidence of the fluctuation of the measured AS (ASA and ESA) and the change of the street width is quite interesting. People may expect the correlation of AS and the transceiver distance (or in other words, the large-scale fading like *path loss*). For example, does AS vary monotonically with the increase of distance? However, our measurement data have shown that the correlation may not be so straightforward as expected by intuition. The phenomena observed may be explained as follows.

For easy presentation, we review the definition of AS first. AS is not concerned with the absolute amount of incident power, but with the angular distribution of power arrival. Specifically speaking, the value of AS depends on the proportion of the arrived power through LOS path and the power through the multipath components (MPCs) which arrive at the receiver from much wider angles. If the former is much larger than the latter, the AS should be small. Otherwise, if MPCs makes considerable contribution in the APS, the AS should be large. More importantly, when the UE is moving to different locations, the variation of AS depends on the change of the proportion of the power through LOS path and through MPCs in the total received power.

The fluctuation of the ASA and ESA in the LOS scenario may be explained as follows.

- In the narrow street (*Area1* and *Area3*), the buildings are close to the UE. The MPCs scattered from the buildings have relatively high power and thus make considerable contribution in the incident power at the BS. When the UE is moving away from the BS, the power arrival through the LOS path and through the MPCs all decrease due to larger path loss. However, since the MPCs are reflected from the surrounding buildings, their power decreases faster than the LOS propagation. Consequently, the proportion of the power contributed by the MPCs in the total arrived power decreases. This results in the decrease of ASA and ESA.
- In the wide street (*Area2* and *Area4*), the buildings on the street sides are far away from the UE and hence the power of the MPCs scattered from the buildings is quite small. In this case, the LOS propagation is dominant. When the UE is moving further away from the BS, the received power through both LOS and MPCs decreases. However, the power from MPCs has already be very small and will not change too much, but the decrease of the LOS power is now more significant compared with that of the MPC power. This leads to the decrease of the proportion of LOS power in the total arrived power. Thus, ASA and ESA become larger.

The analysis above may lead to such a conclusion. In urban street canyon environment with LOS propagation, the ASA and ESA at the BS depends on both the UE distance and the street width. When the street is narrow, both AS will decrease with the increase of the UE-to-BS distance. However, the tendency will reverse in a wide street even in the same scenario.

C. ASA and ESA in NLOS Scenario

The results in NLOS scenario are plotted in Fig. 6. We can see that again both curves run zigzag with the increase of the UE distance. As shown in the map in Fig. 4, the situation of the measurement street is also changing due to the layout of the constructions on the sides. The street can be divided into 5 areas. *Area1*, *Area3* and *Area5* are just in front of and quite closed to three 5-floor buildings, while *Area2* and *Area4* are open areas in the middle of two buildings.

It can be seen that the variation tendency of ASA and ESA in Fig. 6 also matches the situation of the street. In particular, both ASA and ESA increase when the UE was moved in *Area1*, *Area3* and *Area5*, and they decrease in the other two areas. Again, the fluctuation tendency of ASA and ESA are basically coincident with each other. The reasons of AS fluctuation in the NLOS measurement may be as follows.

- First, compared with the ASA and ESA in LOS scenario, the values of NLOS scenario are larger. This is expected because in NLOS case the MPC power makes more significant contribution in the total arrived power than in LOS scenario.
- In *Area1*, *Area3* and *Area5*, the UE is quite close to the buildings in these three areas. With the move of UE inside these areas, it becomes more difficult for the LOS direction propagation to penetrate the building. Since the received power by LOS propagation is attenuated

more severely, its proportion in the total received power decreases and thus the AS increases.

- ASA and ESA decrease in *Area2* and *Area4* where the UE was in the middle of two buildings. Although the LOS path is still obstructed, the "Quasi-LOS" path diffracted over the building roof occurs. It has been reported in several works that this "Quasi-LOS" path contributes considerable received power [4]. The measurements have shown that in LOS scenario, "Quasi-LOS" is usually the secondary significant path only to the LOS path. Therefore, it can be conjectured that the power through this 'Quasi-LOS" path become dominant in the arrived power to the BS. With the UE moving toward south, it is further away from the blocking building, so the propagation through the "Quasi-LOS" path becomes more efficient and thus its power arrived at the BS may increase. Since the power proportion of "Quasi-LOS" path increases considerably, ASA and ESA decrease quickly.

In summary, in NLOS scenario in typical urban street canyon, the existence of "Quasi-LOS" path plays a critical role in determining the tendency of ASA and ESA. In the "hard NLOS" scenario without "Quasi-LOS" path, AS usually becomes larger with the increase of the distance because multipath effect becomes more intensive and the incident angles of the MPCs may be more random. However, when the "Quasi-LOS" path exists and its power becomes stronger, AS may decrease accordingly.

IV. Channel Characteristics Modeling

A. Distribution of ASA and ESA

As presented in Section II, for each UE position, we obtained 16 samples of APS for one polarization and one dimension. Thus, 16 samples of ASA and ESA each can be calculated. For the total 100 UE positions in LOS scenario, we obtained 1600 samples of ASA and ESA each. Similarly, for the NLOS scenario with 95 UE positions, 1520 samples were obtained.

Fig. 7 and 8 plot the empirical distributions of ASA and ESA for the LOS and NLOS scenarios, respectively. The distributions are tested against truncated Gaussian and Laplacian densities and the latter turned out to be a better fit. The superimposed curves are best fit Laplacian PDFs determined by integrating over each bin and matching the histogram using least squares. ASA and ESA of the UMa street channel are modeled by Laplacian distribution, which can be expressed as

$$f_{EAS}(\theta) = \frac{1}{2\sigma_{EAS}} \exp\left(-\frac{|\theta - \mu_{EAS}|}{\sigma_{EAS}}\right), \qquad (4)$$

where μ_{EAS} and σ_{EAS} stand for the mean and standard deviation (STD) for ESA in LOS or NLOS scenario. The PDF expressions for ASA can be specified by replacing the subscript by ASA and the variable θ by ϕ for the convention.

B. Parameters of Laplacian distribution

In this subsection, we would like to determine the mean and STD of the Laplacian distribution of ASA and ESA. First, for

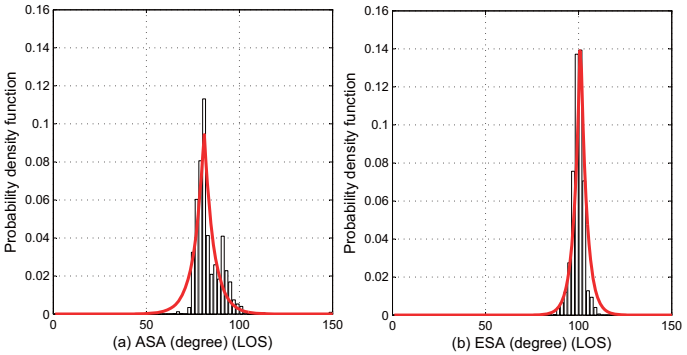

Fig. 7. Distribution of ASA and ESA in LOS scenario. (Superimposed are the best fit Laplacian PDFs.)

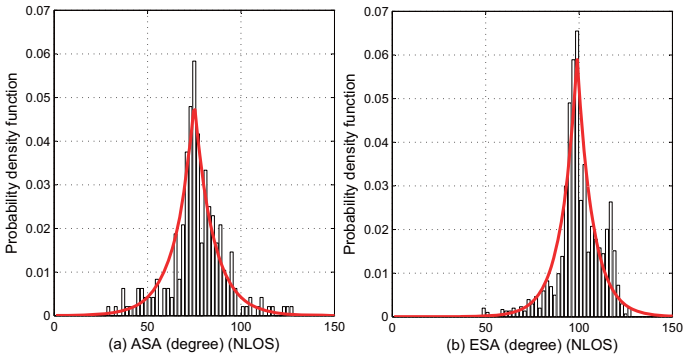

Fig. 8. Distribution of ASA and ESA in NLOS scenario. (Superimposed are the best fit Laplacian PDFs.)

the ESA in LOS scenario, inspired by the zigzag curves in Fig. 5(a), we first model the variation of ESA with respect to UE-to-BS distance in the 5 areas, respectively. We adopt linear regression for the approximation of the mean of ESA, denoted by $\overline{ESA}$. The linear model is

$$\overline{ESA} = A_{E,L,x}d + B_{E,L,x}, \qquad (5)$$

where $A_{E,L,x}$ and $B_{E,L,x}$ are the linear function coefficients and the subscript $\{E, L, x\}$ stands for ESA, LOS scenario and the x-th area ($x = 1, 2, 3, 4$), and d is the distance between the BS and UE. Similarly, we can obtain the linear model of the mean of ASA in LOS scenario, which also corresponds to the 4 areas in Fig. 5(b). The linear regressions for ASA and ESA in NLOS scenario are also defined in the same way, but corresponding to the 5 areas shown in Fig. 4. The coefficients using linear fitting are listed in Tab. I. Please note that we reorder the areas and list the coefficients of the homogeneous areas together for easy reading.

Furthermore, it can be found in Tab. I that the slopes of ASA/ESA linear regression in homogeneous areas are closed to each other. For example, the slopes of *Area1* and *Area3* in LOS scenario, *i.e.*, $A_{E,L,1}$ and $A_{E,L,3}$, are quite close to each other. Thus, we can use the average of the coefficients of homogeneous areas as the final model parameters. The linear regression curves with the averaged slope are plotted in Fig. 5 and 6, where we can see a good match between the model and measurement results even in multiple areas.

TABLE I
VALUES OF LINEAR REGRESSION COEFFICIENTS

Scenario		A_{ASA}	B_{ASA}	A_{ESA}	B_{ESA}	σ^*_{AS}
LOS	*Area1*	-0.08	19.35	-0.12	22.04	$U[0 \sim 2]^o$
	Area3	-0.03	10.55	-0.08	24.50	
	Area2	0.18	-32.7	0.04	-5.61	
	Area4	0.07	-18.8	0.02	-4.54	
NLOS	*Area1*	0.39	-39.5	0.19	-19.4	$U[2 \sim 7]^o$
	Area3	0.36	-79.4	0.14	-32.7	
	Area5	0.13	-19.6	0.15	-46.7	
	Area2	-0.35	89.6	-0.10	30.4	
	Area4	-0.44	176.7	-0.19	75.1	

σ^*_{AS} means the values listed below are applicable to both ASA and ESA.

The modeling above indicates that we may divide the LOS street environment into two cases, the "narrow street LOS" and "wide street LOS". In the former, the power of MPCs changes dramatically with the location of the UE, and thus the AS decreases with the increase of transceiver distance. However, in the latter, the power of MPCs changes not so dramatically and thus the AS increases with the increase of transceiver distance.

For the NLOS scenario, we may divide the NLOS street environment into two cases too. One is the "hard street NLOS" and the other is "soft street NLOS". The former means that the UE is too closed to a building to have the "Quasi-LOS" path. In this case, ASA and ESA will increase with the increase of the transceiver distance, as discussed in Section III-C. The latter means that the "Quasi-LOS" path exists and becomes much more significant than the other MPCs. In this case, the AS will decrease with the increase of the power through the "Quasi-LOS" path. The slope of mean ASA and ESA in these two NLOS cases can also be obtained by taking the average of the measurement results in the corresponding areas.

Finally, the averaged values of the STD, σ_{AS}, at different distances are plotted in Fig. 5 and 6 for LOS and NLOS scenarios, respectively. It can be seen that the STD does not show clear dependency on the UE position and street situation. Instead, the STD samples vary slightly and randomly within the range of about $[0 \sim 2]^o$ and $[2 \sim 7]^o$ for LOS and NLOS scenarios, respectively. Therefore, we propose to model σ_{ASA} and σ_{ESA} by uniform distribution inside these ranges.

V. CONCLUSION

For an assessment of the true potential and performance of 3D MIMO systems, measurements of full spatial channels are a prerequisite. In this paper, a field 3D channel measurement campaign was carried out in UMa typical street canyon environment. A measurement technique based on two UPA antennas and a wideband channel sounder was applied to characterize the angle-of-arrival at the BS. The UE (Tx) was located at different distances away from the BS. Interesting observations on the variation of ASA and ESA are found. The expected simple correlation between AS and large-scale fading may not be true, because AS is determined by the proportion of the power from LOS or "Quasi-LOS" path and the power from MPCs. In LOS scenario, the distance and the street width are both key factors in determining the mean of ASA and ESA. When the UE is moving away from the BS in narrow street, the AS will decrease, indicating that the arrived power at the BS through MPCs is decreasing faster than that through LOS propagation. However, the tendency is reversed in wide street. In NLOS scenario, the power through "Quasi-LOS" path diffracted over the building roof determines the AS. If the "Quasi-LOS" power is increasing, the AS will decrease, and vice versa. This also depends on the specific environment of the street. We have also demonstrated that the randomness of ASA and ESA can be modeled by Laplacian distribution. The results in this paper might indicate the direction of how to extend current 2D channel models such that they can eventually be used for the realistic 3D channel simulations.

The interesting observations in this paper beckons for more field measurements in various environments and verification of the 3D spatial model. Furthermore, when antenna arrays are introduced at mobile stations of cellular networks, accurate modeling of the spatial radio channel at the UE side will become also crucial.

ACKNOWLEDGEMENT

The authors would like to thank the Huawei research fellows, Dr. J. Li and Dr. P. Yang, for their great help with the development of the hardware/software of the channel sounder, and Dr. J. Liu and Dr. J. Wang, for their fruitful technical discussions on spatial parameter estimation. This work was partly supported by NSFC (61202394), NCET of China, NPU Fundamental Research Program, Higher Education Doctoral Program Foundation (20116102120030) and the Foundation for Selected Chinese Oversea Scholars.

REFERENCES

[1] 3GPP, "Spatial channel model for multiple input multiple output (MIMO) simulations (release 7)," Tech. Rep. Technical Specification Group Radio Access Networks, TR 25.996, v7.0.0, Jun. 2007.

[2] WINNER, "Winner II channel models," Tech. Rep. IST-4-027756 WINNER II, D.1.1.2 V1.2, Sep. 2007.

[3] J. Fuhl, J.-P. Rossi, and E. Bonek, "High resolution 3-D direction-ofarrival determination for urban mobile radio," *IEEE Trans. Antennas Propag.*, vol. 45, no. 4, pp. 672–682, Apr. 1997.

[4] A. Kuchar, J. P. Rossi, and E. Bonek, "Directional macro-cell channel characterization from urban measurements," *IEEE Trans. Antennas Propag.*, vol. 48, no. 2, pp. 137–146, Feb. 2000.

[5] N. Jalden, P. Zetterberg, and B. Ottersten, "Directional dependence of large scale parameters in wireless channel models," in *Proc. IEEE WCNC'08*, Mar. 2008.

[6] K. Kalliola, H. Laitinen, P. Vainikainen, M. Toeltsch, J. Laurila, and E. Bonek, "3-D double-directional radio channel characterization for urban macrocellular applications," *IEEE Trans. Antennas Propag.*, vol. 51, no. 11, pp. 3122–3133, Nov. 2003.

[7] K. Kalliola, K. Sulonen, H. Laitinen, O. Kivekas, J. Krogerus, and P. Vainikainen, "Angular power distribution and mean effective gain of mobile antenna in different propagation environments," *IEEE Trans. Veh. Technol.*, vol. 51, no. 5, pp. 823–838, Sep. 2002.

[8] J. Medbo, H. Asplund, J.-E. Berg, and N. Jalden, "Directional channel characteristics in elevation and azimuth at an urban macrocell base station," in *Proc. 6th European Conference on Antennas and Propagation (EuCAP'12)*, Prague, Mar. 2012.

[9] Q. Spencer, B. Jeffs, M. Jensen, and A. Swindlehurst, "Modeling the statistical time and angle of arrival characteristics of an indoor multipath channel," *IEEE J. Sel. Areas Commun.*, vol. 18, no. 3, pp. 347–360, Mar. 2000.

[10] J. Wang, S. Wang, and R. Zhang, "A fast iterative two-dimensional MUSIC algorithm for angle-of-arrival estimation," Northwestern Polytechnical University, Xi'an, Shaanxi, China, Tech. Rep., Sep. 2013.